

The impact of room location on time reversal focusing amplitudes

Brian D. Patchett, Brian E. Anderson, and Adam D. Kingsley

Citation: *The Journal of the Acoustical Society of America* **150**, 1424 (2021); doi: 10.1121/10.0005913

View online: <https://doi.org/10.1121/10.0005913>

View Table of Contents: <https://asa.scitation.org/toc/jas/150/2>

Published by the *Acoustical Society of America*



**Advance your science and career
as a member of the**

ACOUSTICAL SOCIETY OF AMERICA

LEARN MORE



The impact of room location on time reversal focusing amplitudes

Brian D. Patchett, Brian E. Anderson,^{a)} and Adam D. Kingsley

Acoustics Research Group, Department of Physics and Astronomy, Brigham Young University, Provo, Utah 84602, USA

ABSTRACT:

Time reversal (TR) is a signal processing technique often used to generate focusing at selected positions within reverberant environments. This study investigates the effect of the location of the focusing, with respect to the room wall boundaries, on the amplitude of the focusing and the uniformity of this amplitude when focusing at various room locations. This is done experimentally with eight sources and two reverberation chambers. The chambers are of differing dimensions and were chosen to verify the findings in different volume environments. Multiple spatial positions for the TR focusing are explored within the rooms' diffuse field, against a single wall, along a two-wall edge, and in the corners (three walls). Measurements of TR focusing at various locations within the room show that for each region of study, the peak amplitude of the focusing is quite uniform, and there is a notable and consistent increase in amplitude for each additional wall that is adjacent to the focal location. A numerical model was created to simulate the TR process in the larger reverberation chamber. This model returned results similar to those of the experiments, with spatial uniformity of focusing within the room and increases when the focusing is near adjacent walls. © 2021 Acoustical Society of America. <https://doi.org/10.1121/10.0005913>

(Received 27 April 2021; revised 24 June 2021; accepted 30 July 2021; published online 25 August 2021)

[Editor: Julien de Rosny]

Pages: 1424–1433

I. INTRODUCTION

Time reversal (TR) is a signal processing technique that relies on the principle of reciprocity in a given environment to generate a focused signal at a location within that environment.^{1,2} This technique benefits from being performed in a reverberant environment and is often performed in one. It began as a method called matched signal processing for underwater communication^{3–5} and has since branched to multiple scientific fields such as medicine,^{6,7} nondestructive evaluation of materials (NDE),^{8–10} and source event localization in geophysics.¹¹ TR has also been explored with sound in the audible range as a method of communication in complex reverberant environments^{12,13} as well as common room situations.¹⁴ Recently, TR of high-amplitude ultrasound in air was used to generate a difference frequency.¹⁵ The focusing process is comprised of two steps, an initial forward step in which the impulse response (IR) of the environment is calculated and a backward step where the IR is reversed in time and broadcast from the initial source position [the so called reciprocal TR (Ref. 2) process]. This time reversed impulse response (TRIR) signal is then broadcast, causing energy to converge on the receiver position, resulting in impulsive focusing.

To achieve the forward step of TR, multiple sources and a single receiver are placed in a reverberation chamber. A chirp signal is broadcast from each of the source locations individually, and the chirp response (CR) of each broadcast is recorded at the receiver position. Because the IR is spatially unique for each individual source/receiver system, this step is performed

consecutively for each of the eight sources alone. If the IRs were not captured consecutively, then the signal recorded at the receiver would be a mix of all eight IRs together, and they could not be separated for the backward step performed later. This also produces individual IRs with better resolution and signal-to-noise ratio than if they were all collected simultaneously. The CR is described mathematically as the convolution of the chirp signal with the IR of the reverberation chamber. Once the CRs have been recorded, the IR for each can also be calculated. Once obtained, the IR is reversed on the time axis, creating the TRIR. Each of the TRIRs is then broadcast from all sources simultaneously. Due to the reciprocal nature of the system, the emissions from the TRIRs from each source trace the same paths back through the reverberation chamber to the receiver. The result is a convergence of the signals on the receiver, generating a focus. The location of this focusing will be termed the focal location. The converging acoustic waves behave in such a way that the eight simultaneous broadcasts overlap constructively and add collectively to the focusing amplitude. The amplitudes are such that linearity can be assumed in each individual chirp broadcast, but during the backward step the amplitude of the converging waves near the focal location is large enough that nonlinear phenomena occur. In the medical field, a similar TR technique is employed to both locate and destroy kidney stones in a technique known as lithotripsy.^{7,16} Scientists studying NDE have employed this method of TR in solids to evaluate damage to a material through vibrational excitation of the material using a TR generated focus in this same way.^{9,10}

The first studies applying TR to room acoustics focused primarily on communication in reverberant environments

^{a)}Electronic mail: bea@byu.edu, ORCID: 0000-0003-0089-1715.

with complex structures. Candy *et al.*^{12,13} studied the application of TR communication in highly reverberant environments. They found that communication quality could be improved through the use of multiple sources and a linear equalization filter. In a subsequent study, Ribay *et al.*¹⁷ applied a room acoustics model, based on work by Draeger and Fink¹⁸ and Derode *et al.*¹⁹ using TR in solid materials, to show that focal amplitudes are dependent upon the number of sources present, the reverberation time (RT_{60}) of the environment, and the bandwidth of the IR. Additionally, Yon *et al.*¹⁴ performed an experimental study in a standard room (non-reverberation/non-anechoic), finding that TR produces temporal and spatial focusing that is better than time-delay beamforming. This is due to multiple sound paths between the sound sources and focus location. It was also found that increasing the number of sources while simultaneously increasing the bandwidth of the IR decreases the level of the side lobes, resulting in improved focusing. Those experiments were done with a linear 20-loudspeaker array and a single microphone mounted to a linear scanning system. This allowed the group to measure the focus both spatially and temporally. A numerical and experimental study recently conducted by Denison and Anderson^{20,21} was able to show through similar modeling techniques that changes in RT_{60} due to changes in the volume of the room affect the amplitude of the focus differently than do changes to absorption. Increasing the volume of a reverberant environment (thereby increasing RT_{60}) with similar boundary conditions (wall absorption) leads to a decrease in peak focal amplitudes when all other variables remain constant. They were also able to show a direct connection between the RT_{60} of a room and the performance of the TR focusing, demonstrating that a longer RT_{60} reduced the spatial side lobes that are characteristic to TR focusing. Their experimental work was done in a reverberation chamber, where absorbers were used to tailor the RT_{60} to study the effect on the focus signal. Ribay *et al.*¹⁷ limited their study to changes in RT_{60} due to changes in absorption (they did not explore the impact of room volume). Denison and Anderson verified the work of Ribay *et al.*, while also studying the impact of a changing volume. However, Denison and Andersons' experimental verifications of the increased volume effect were limited to non-ideal environments. These effects have not been studied or verified in reverberation chambers until now. Experimental work performed by Ma *et al.*²² found that when using metamaterial objects known as acoustic prisons, they were able to increase the peak focus intensity when additional reverberating surfaces were included inside of the prison objects. Additional work by Ma *et al.*²³ used a set of loudspeakers with a microphone and reported findings similar to those discussed above, primarily that chirp bandwidth, chirp time duration, and RT_{60} all affect the focus in a meaningful way.

Previous studies have not explored the impact of the TR focal location's position within a room (i.e., near walls or away from walls and what level of consistency is found when away from walls) on the TR focusing amplitude. The

purpose of this paper is to apply the TR process experimentally in two different reverberation chambers, along with numerical modeling of TR in a reverberation chamber, to show how the TR focusing amplitude depends on the focal location within a room. Reliable prediction of an expected focus amplitude at a given position within the environment relative to reflecting surfaces is necessary when applications involve using TR to deliver energy to that position. Resulting data show that the amplitude increases by moving the focal location from a diffuse field position (away from all walls/surfaces) to a position adjacent to one reflecting wall by approximately 3 dB. In this paper, the word "wall" will be used to refer to any of the four walls, the ceiling, or the floor. It increases again near a two-wall edge and again in the corner of the room where three walls are adjacent to the focal location. The increase in amplitude for diffuse sound in a room is well known to be a 6 dB increase with each additional reflecting surface. A mathematical description of the TR process is performed in Sec. V, confirming that the resulting increases should also be on the order of 6 dB, and a reason why they are not that high in both the experiment and the model is given. The amplitude of the focusing is also quite uniform when the focal location is placed anywhere within the diffuse field of the room. This is in contrast to the expected outcome for diffuse sound fields in rooms, where one standard deviation away from the mean of the level can be expected to vary by as much as +5/−6 dB.²⁴ The volume of the room has a significant effect on the amplitude as well, confirming the results obtained by Denison *et al.*²⁰ The measurements taken in the small reverberation chamber (SRC) were consistently higher than those taken in the large reverberation chamber (LRC) when using the same configuration and output settings.

It is worth noting that the peak sound pressure levels (SPLs) attained in the experiments presented here were on the order of 150–160 dB. These are only peak levels of a short duration focal event, but these levels are considerably high. Applications for these levels include the investigation of high amplitude sound acting on rigid bodies, testing of hearing protection at high amplitudes, and use as a tool to study nonlinear sound propagation. The work of Willardson *et al.*²⁵ showed that nonlinear effects can begin to cause distortion in the TR focusing when the peak levels exceed about 160 dB. Thus, we assume that the peak levels reported here are within the linear regime.

II. EXPERIMENTAL DETAILS

A. Setup

The experiments were conducted in two separate reverberation chambers. The two chambers were chosen because they differ in volume but have similar construction. The walls, floors, and ceilings are composed of the same materials and treatment from one chamber to the next. And there are diffuser panels of similar material suspended in each. Dimensions of the SRC are 5.70 m × 4.30 m × 2.50 m, with a volume of 61.3 m³. The SRC has an overall RT_{60} of 4.2 s,

with a Schroeder frequency of 522 Hz. The LRC measures $4.96\text{ m} \times 5.89\text{ m} \times 6.98\text{ m}$, with a volume of 204 m^3 , an overall RT_{60} of 7.6 s averaged across the frequency spectrum of the input signal,²⁶ and a Schroeder frequency of 410 Hz.²⁷ A GRAS (Holte, Denmark) 40BE free-field microphone with a 26CB preamplifier is used as the receiver (referred to as a microphone in this section) with a GRAS 12AX power module. BMS (Hannover, Germany) 4590 dual diaphragm high output loudspeakers fitted with original equipment manufacturer (OEM) crossovers and horns are utilized as the sources (referred to as loudspeakers in this section). It was found by Anderson *et al.* that directionality of sources has a destructive effect on the focus amplitude when the sources are pointed at the focal location and that facing the sources away from the focal location serves to increase the focus amplitude.²⁸ As such, these loudspeakers are placed near the walls in the room and oriented in such a way as to be facing away from the focal location (microphone position) (see Fig. 1). Two four-channel Crown (Stamford, CT) CT4150 amplifiers are used to provide power to the loudspeakers. All signals are generated and processed for TR using a custom in-house LabVIEWTM interface, coupled with two Spectrum (Grosshansdorf, Germany) M2i.6022 signal generation cards and an M2i.4931 digitizer card. All post-processing is handled in MATLABTM.

To begin, a logarithmic chirp signal with a bandwidth of 500–15 000 Hz is broadcast from a single loudspeaker, and the CR is recorded at the microphone position. In initial trials, the use of a logarithmically swept chirp signal produced a higher amplitude focus than a linear chirp signal. It was found by Willardson *et al.* that extending the bandwidth beyond 500–7500 Hz had a negligible effect on the peak amplitude of the focus in the LRC environment.²⁵ However, the Willardson study was limited in that the equipment only had the capability of reaching 9500 Hz. The drivers used in the current study have been upgraded with OEM crossovers, allowing for frequencies up to 15 000 Hz. Since the objective of this study, in part, is to produce a focus with a high signal-to-noise ratio, the decision to extend the bandwidth to the full flat frequency response capability of the driver

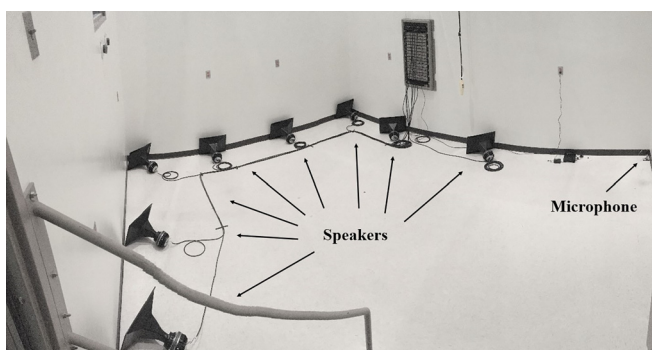


FIG. 1. (Color online) Photograph of the experimental layout in the LRC. The room is a rectangular room with parallel walls, along with reflecting panels (not shown in the image) intended to make the sound field more diffuse. Distortion in the image is due to the panoramic nature of the photograph.

(500–15 000 Hz) was made in order to capture the most possible energy from the focusing sound field.

An IR for this loudspeaker and microphone combination is then calculated using a cross correlation of the chirp with the CR^{28,29} and stored for that loudspeaker channel. This is repeated for each loudspeaker-microphone combination to acquire eight individual IRs. The IRs are then reversed in time to create a set of eight TRIRs, at which point TRIRs are broadcast simultaneously from each of their respective loudspeakers (see Fig. 2). Each IR has a sampling frequency of 250 kHz for the entire process. The high sampling frequency ensures that the peak amplitude of the focusing is captured with high accuracy.

The TR process time aligns the convergence of multiple arrivals of sound to achieve constructive interference in the form of high amplitude focusing of sound at the microphone location. The use of software synchronization of the broadcasts from multiple loudspeakers generates a higher amplitude focus than a single loudspeaker would when used alone. This full TR process is repeated at various spatial positions within the room in this study to explore the dependence of the TR focusing amplitude with respect to the spatial location of that focusing within the room. All measurements are made assuming linearity both acoustically and in terms of the operating limits of the equipment used. Even though the focus amplitude peaks have levels of around 150 dB, linear scaling of the focusing is observed using different amplification levels.²⁴

B. Spatial position measurements

One aim of creating a diffuse field in room acoustics is to provide uniform SPLs measured at any location within that diffuse field. However, in Fig. 2.17(a) of Kleiner and Tichy²⁴ and in Fig. 3.8 of Kuttruff,³⁰ it is demonstrated that the pressure values measured across a diffuse field in a reverberant room can vary by greater than $\pm 10\text{ dB}$ for a given frequency as a measurement receiver is moved across the space. Kleiner and Tichy quantified the variation by stating, “The logarithmic representation of twice the variance that contains 70% of the sound amplitudes is (nonsymmetrically) within 11 dB...”.²⁴ In other words, 70% of the pressure fluctuations can be within +5 or -6 dB above and below the mean value (one standard deviation above and below the mean).

This variation is due to modal overlapping throughout the space, even though the frequency range may be above the Schroeder frequency.³¹ It is therefore interesting to investigate how the amplitude of TR focusing varies across the diffuse field region of a room and how the proximity of the focal location to walls impacts the amplitude of the focusing. It may be of interest to know how much uncertainty in the focusing amplitude one might expect when using TR to focus sound to a given location within a room. Throughout these measurements, it is useful to keep in mind that the focal location is changed by moving the microphone to different locations in the room, while keeping the

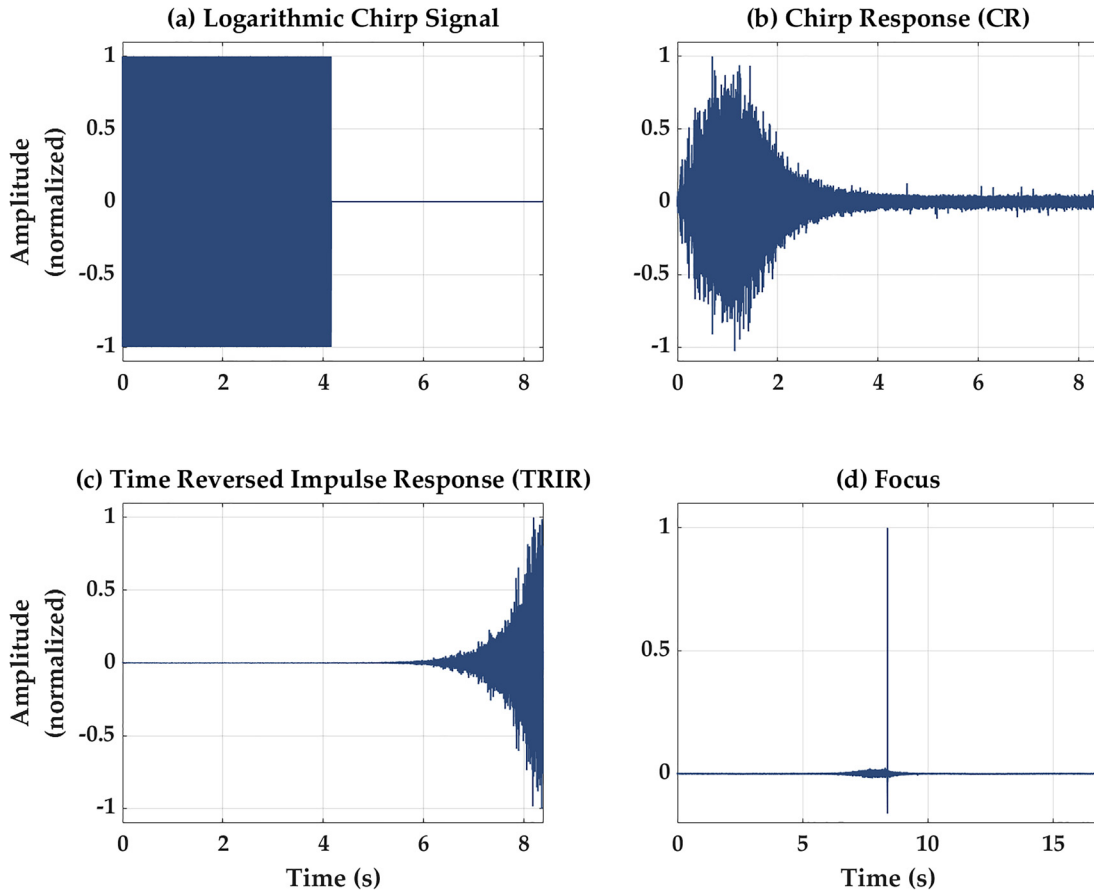


FIG. 2. (Color online) example signals used in the TR experiments. (a) The logarithmic chirp signal, 4.16 s in length. (b) The CR recorded in the forward process at the microphone. (c) The normalized TRIR. (d) Focus generated by simultaneous broadcast of eight loudspeakers. All amplitudes in this figure are normalized for clarity in display.

loudspeakers' locations fixed, and redoing a full TR experiment at the new microphone location (both forward and backward steps).

The various focal locations explored here include four different types of locations, with focal locations of similar types being referred to as regions: the open space (diffuse field region) of the room, against one of the reflecting walls (wall region), against two of the reflecting walls (edge region), and against three walls of the room (corner region). The diffuse field position measurements are made in accordance with the ISO standard,³² where a diffuse field is defined as occurring at least 1 m from any reflecting wall. A total of 20 diffuse field focal locations are chosen at random, while ensuring that the focal location is at least 1 m from any of the reflecting walls in the room (see Fig. 3). The single wall measurements are made at six random positions against one of the reflecting walls in the room. Care is taken to ensure that the focal location remains more than 1 m from any other adjacent wall. The edge region measurements are made at six locations in the room. Again, care is taken to keep the focal location at least 1 m away from the corners of the room. For practical purposes, only four corner measurements are made due to the geometry of the rooms and the difficulty in reaching the upper corners reliably with the microphone. In the one- and two-wall region measurements,

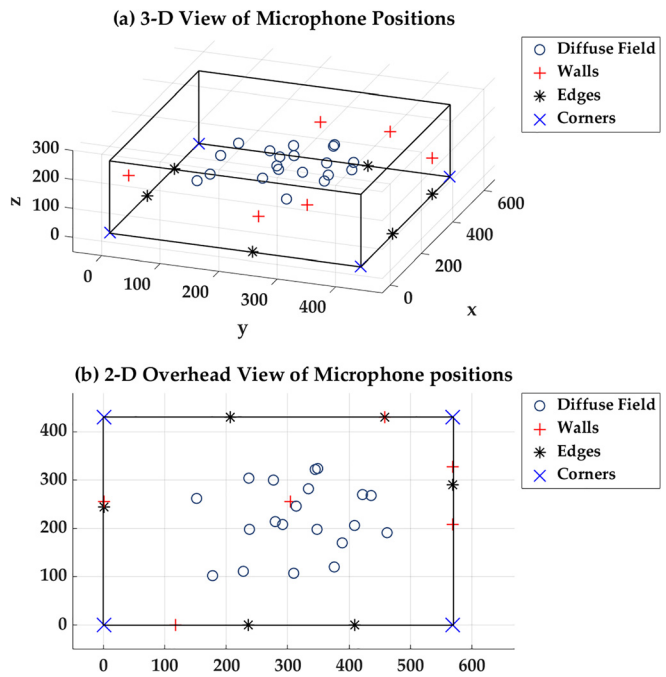


FIG. 3. (Color online) Microphone positions in the SRC. Each position region is denoted with a unique character. (a) Three-dimensional (3-D) representation of positions. (b) Top-down view of the chamber in two dimensions (2-D).

the microphone is placed 1 cm from any wall for consistency in positioning. The body of the microphone is oriented so that it is parallel to the walls. In the case of the corner measurements, the microphone is pointed directly into the corner, 1 cm from its apex, with an equal angular alignment from each wall. Measurements are performed in both the SRC and LRC to compare results for both environments.

Figure 4 illustrates the focal amplitude measurements with a bar graph in decibels (peak SPLs). This figure shows clearly that the position of the focal location in proximity to additional walls has a consistent effect of increasing the focusing amplitude. It is also worth noting that the focusing amplitude in each particular region has very little variance from the mean SPL. This indicates that there is a fair amount of uniformity of the focusing amplitude at various focal locations within the same region, especially when compared to the greater than ± 10 dB fluctuations that can be expected when moving a microphone to various locations within a diffuse field without using TR. This means that one can reliably expect a certain focal amplitude irrespective of where they choose to focus sound with TR within a given region of the room.

The mean values in Fig. 4 were calculated using the squared pressure values, as this accurately represents the energy relation to the peak focal amplitude values in the sound field. Standard deviations were measured as 150.5 dB (+0.5/-0.5 dB) in the diffuse field, 153.6 dB (+0.8/-1.0 dB) against one wall, 155.7 dB (+0.9/-1.0 dB) against an edge (two walls), and 158.7 dB (+0.7/-0.8 dB) for the corners (three walls), where the values in the parentheses represent one deviation above and below the mean pressure value. As is evident in the mean values reported, the average focusing amplitude for a focal location near a wall increases by 3.1 dB (+0.6/-0.7 dB) from the diffuse field focal locations. The average increases again by 2.1 dB (+0.7/-0.8 dB) when the focal location is placed near an edge (two walls) compared to one-wall focal locations. Corner locations (three walls) again increase the focusing amplitudes by 3.0 dB (+0.6/-0.7 dB) relative to an edge (two walls).

The variation of the focal locations for TR experiments conducted in the SRC is now similarly conducted in the LRC. All signal settings, gain values, and signal processing

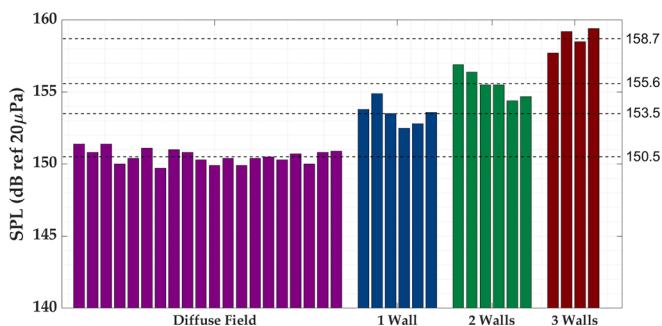


FIG. 4. (Color online) Bar graph display of measured peak SPL for various TR experiments done at the locations specified in Fig. 3 for the SRC. The mean of the peak SPL values for each region is displayed as a dashed line with mean value label to the right.

are identical to those used in the SRC experiments to ensure a direct comparison between the two rooms of different volumes. The set of measurements made in the LRC also serves to confirm that the results from the SRC may be expected in other similar rooms and allows for comparison of the focusing amplitudes in two similar rooms of different volumes. Figure 5 shows the microphone positions used to measure peak focal amplitudes in the LRC, while Fig. 6 shows a similar bar graph as Fig. 4, but now for values measured in the LRC.

A similar uniformity is observed in the LRC measurements as was observed in the SRC measurements for each region of locations. The mean value (and one standard deviation above/below the mean) was measured to be 147.7 dB (+1.0/-1.4 dB) in the diffuse field, 151.5 dB (+0.4/-0.5 dB) against one wall, 153.7 dB (+0.7/-0.8 dB) against an edge (two walls), and 156.1 dB (+0.5/-0.6 dB) for the corners (three walls). Here, the mean diffuse field peak focal amplitude increases by 3.8 dB (+1.0/-1.2 dB). Moving to an edge, the mean increases by 2.2 dB (+1.0/-1.2 dB). Moving from an edge to a corner, the mean increases by 2.4 dB (+0.9/-1.1 dB). According to the experimental data, the SRC consistently yields higher focusing amplitudes regardless of the type of location within the room. For example, the focusing amplitude at SRC diffuse field focal locations is consistently higher than the focusing amplitude at LRC diffuse field focal locations. This agrees with the finding of Denison *et al.*²⁰ that, when all other experimental characteristics are kept the same, the smaller volume room will have a higher TR focusing amplitude. Figure 7 shows a comparison of the

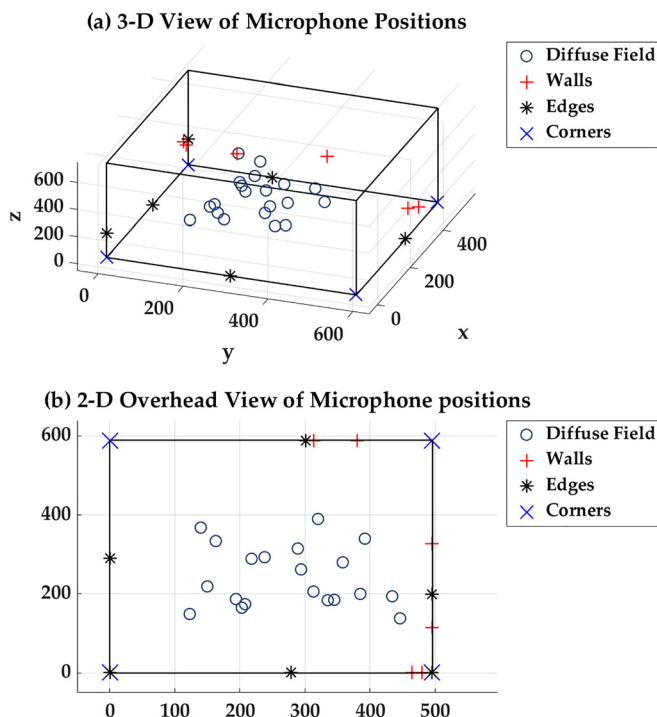


FIG. 5. (Color online) Microphone positions in the LRC. Each position region is denoted with a unique character. (a) 3-D representation of positions. (b) Top-down view of the chamber in 2-D.

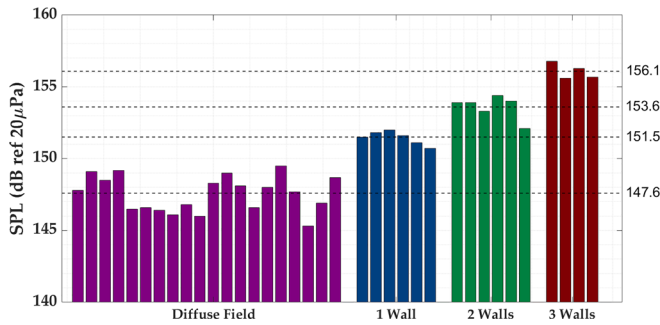


FIG. 6. (Color online) Bar graph display of measured peak SPL for various TR experiments done at the locations specified in Fig. 5 for the LRC. The mean of the peak SPL values for each region is displayed as a dashed line with mean value label to the right.

averaged focal signals measured at the focal locations in the SRC and LRC (averaged across the focal locations within a given region for a given room). This illustrates that the increase in peak focal amplitudes is consistent for the measurements performed in the SRC versus the LRC.

III. NUMERICAL MODEL OF EXPERIMENT

A numerical model was generated to compare the experimental results obtained in the LRC to theory. The model is based on a modal summation equation given by Kleiner and Tichy.²⁴ This form of modal summation as a way to model TR differs from both Denison and Anderson^{20,21} and Ribay *et al.*,¹⁷ who each used models based on geometric ray tracing and image sources. Denison and Anderson²⁰ used an image source model of TR in a room, and though they did not report this in their paper, they did not observe an increase

in TR focusing amplitude when focusing near walls in their model. As such, a new method that incorporated the summation of pressure contributions from each excited mode in the reverberation chamber was deemed appropriate in an attempt to match observed experimental results. The model here assumes a rectangular room with parallel walls. The presence of diffusors is not factored into the calculation, though they are present in the experimental reverberation chambers.

The equation describes the pressure, \hat{p} , at receiver position (x, y, z) due to any given source position, (x_0, y_0, z_0) , as a function of frequency or wavenumber, k , in a 3-D environment. It is a frequency response between the source and receiver locations,

$$\hat{p}(x, y, z, k) = -4\pi \frac{A}{V} \sum_{n=0}^{\infty} \frac{\Psi_n(x_0, y_0, z_0) \Psi_n(x, y, z)}{(k^2 - k_n^2 - j2k_n \frac{\delta_n}{c}) \Lambda_n}, \quad (1)$$

where A is the monopole amplitude related to the source strength (or volume velocity), Q , used in the original equation through the relationship,

$$A = \frac{j\rho_0 ckQ}{4\pi}, \quad (2)$$

V is the room volume (204 m^3), n is the mode number, Ψ_n is the spatial dependence of the n th mode, k_n is the wavenumber for the n th mode, and δ_n is the damping factor. Λ_n is the function that accounts for orthogonality such that

$$\Lambda_n = \frac{1}{\epsilon_{n_x} \epsilon_{n_y} \epsilon_{n_z}} \quad \text{and} \quad \epsilon_{n_x, n_y, n_z} = \begin{cases} 1, & \text{for } n_x, n_y, n_z = 0 \\ 2, & \text{for } n_x, n_y, n_z = 1 \end{cases}, \quad (3)$$

where ϵ_{n_x, n_y, n_z} represents the Neumann orthogonality factor for the three Cartesian spatial dimensions. Λ_n can have values of $1/2$ (for axial modes), $1/4$ (for tangential modes), and $1/8$ (for oblique modes). Since the primary purpose of this analysis was the comparison of focal amplitudes obtained at different regions of the room, the amplitude, A , of the source was set to a value of 1 in Eq. (1), resulting in a Green's function. The source output levels can be arbitrary in magnitude since linearity is assumed and only relative increases in focal amplitudes are of interest as they pertain to the focal location region in which they are calculated (diffuse field, wall region, etc.).

The model implies that for a given k , the modal response due to the source position, $\Psi_n(x_0, y_0, z_0)$, and due to the receiver position, $\Psi_n(x, y, z)$, is determined from a summation of an infinite number of normal modes of the room. For the rigid walled room being modeled, with dimensions $L_x = 4.96 \text{ m}$, $L_y = 5.89 \text{ m}$, $L_z = 6.98 \text{ m}$, the eigenfunction can be written as $\Psi_n(x, y, z) = \cos(n_x \pi x / L_x) \cos(n_y \pi y / L_y) \cos(n_z \pi z / L_z)$. As an infinite number of modes would lead to an infinite computation time, only modes whose modal frequencies lie within the bandwidth of 500–15 000 Hz were used, as this is the same bandwidth of

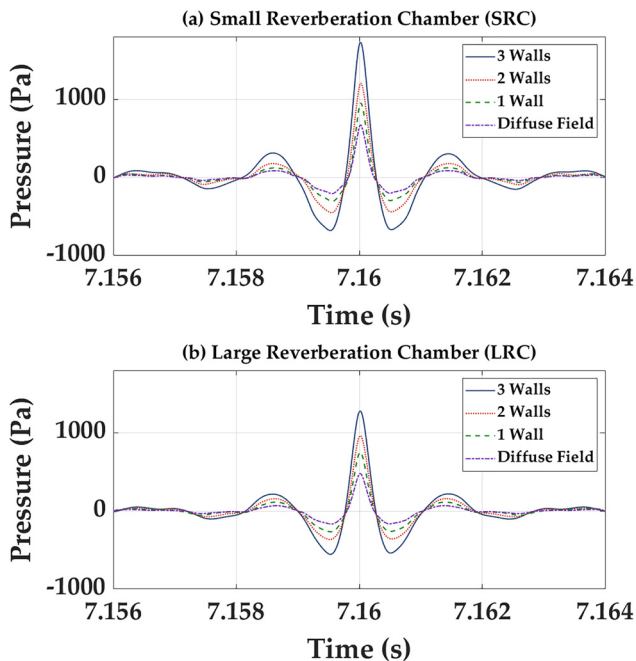


FIG. 7. (Color online) Average focal signals shown zoomed in on the time axis. (a) Comparison of the mean focal signals for each region in the SRC; (b) the same for the LRC.

the chirp used in the experimental data. The modal frequency bandwidth, $\Delta f = 2.2/RT_{60}$ [see Eq. (3.43) of Ref. 30], was calculated for the lowest frequency of the chirp (with the longest RT_{60}) and determined to be 0.44 Hz. Thus, a spacing less than that of $\Delta f = 0.44$ Hz was selected to make sure that every mode would be sampled at this frequency resolution. This means that the calculation for the pressure at each position used a wavenumber value of $k = 2\pi f/c$, where k ranged from $f = 500.25$ Hz to $f = 15\,000$ Hz in steps of 0.25 Hz. This resulted in 60 000 values of k for each spatial position. Given the maximum frequency used, the number of modes summed for each value of k is approximately 7.1×10^7 . While it is possible to limit the number of modes in the summation by including only those with a significant contribution to the pressure amplitude (such as only summing the modes within a certain number of modal bandwidths of a given k), this calculation included all available modes. The damping factor,

$$\delta_n = \frac{6.91}{(RT_{60})_{f_n}}, \quad (4)$$

is calculated from frequency-dependent, experimentally obtained RT_{60} values.³⁰ The frequency-dependent $(RT_{60})_{f_n}$ is calculated using reverse Schroeder integration (RSI) on the IRs measured in the LRC.³³ This ensures that the model has a RT_{60} (and a subsequent δ_n) that matches the experimental values as closely as possible. Before applying the RSI, each IR was filtered using a one-third octave band filter to find the RT_{60} as a function of frequency. The one-third octave values were then linearly interpolated to represent an approximation of the RT_{60} over all discrete frequencies at a resolution of 0.25 Hz, which is the frequency spacing of the model variable f_n . The δ_n values are computed from the extracted values of $(RT_{60})_{f_n}$. This 0.25 Hz resolution was empirically determined to be sufficient. During post-processing, $(RT_{60})_{f_n}$ values were extracted from numerically generated IRs using the RSI method again. This analysis returned $(RT_{60})_{f_n}$ values matching the input $(RT_{60})_{f_n}$ values, indicating that Eq. (4) generates a numerical IR that closely matches the experimentally measured IR.

Due to the quantity of the calculations required for this modeling approach and the size of the data stored in random access memory (RAM) as the pressure is calculated, Eq. (1) is computationally broken down into several pieces and then reassembled for a final calculation (parallelization of the code). This method reduces computation time to one-third of the original time as compared to a non-parallelized version of the code. The k_n^2 and k_n values in the denominator are calculated in a standard “for” loop nested for each physical dimension. Then the product of the eigenfunctions in the numerator is calculated in a parallelized “for” loop (parfor function in MATLABTM) for each index value of x , y , and z . Finally, all of the pieces are brought together into the final form of Eq. (1). The solution for each n value and the summation is computed using the graphical processing unit. The array of pressures at each mode is then summed for each k

value and saved as a pressure versus frequency spectrum. This is repeated for each receiver position, $\Psi_n(x, y, z)$, of interest.

A post-processing modification to the output pressures of the model is used to simulate the experimental use of a logarithmic chirp weighting to the input signal. The weighting was determined by applying a low pass filter with a logarithmic frequency roll-off for the 500–15 000 Hz frequency bandwidth and then determining the appropriate filter values through a curve fit. To simulate a TR focusing of energy, an inverse fast Fourier transform is calculated with the pressure versus frequency vector output from Eq. (1), producing an IR from the numerical model. An autocorrelation of the numerical IR is used to produce a focal signal like that found using standard experimental TR for the given pressure spectrum at that position.³⁴ The application of autocorrelation on the numerical IR ensures that a central data point is always at the exact time for peak of the focus signal, producing a highly accurate value of peak focal amplitude. Because the maximum frequency is 15 kHz, a sampling frequency of 30 kHz is assumed for all focus generation with the numerical data. Example spectra and signals at each step in this simulation of TR can be seen in Fig. 8.

It is worth pointing out that Eq. (1) is the same equation used by Kleiner and Tichy²⁴ to determine the fluctuations in pressure found within a diffuse field. Due to the computational nature of this work, many more focal locations were included in this numerical analysis than were used experimentally. A total of 18 randomized focal locations in each region were selected except for the corners, where seven focal locations were selected. A single source was used in the model for simplicity and economical use of computation time. Its location was chosen to be the lower corner of the numerical “room,” opposite the majority of the measurement locations. Figure 9 depicts the source and receiver positions used as focal locations in the numerical

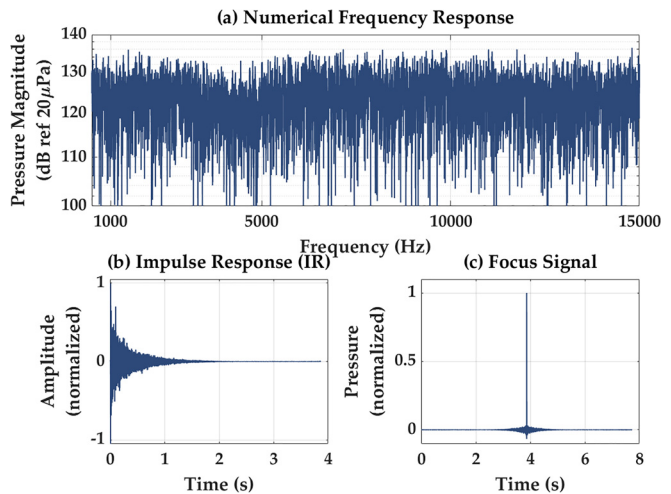


FIG. 8. (Color online) (a) An example frequency response output from the numerical model based on Eq. (1); (b) the IR found by taking an inverse fast Fourier transform of (a); (c) the focal signal generated by an autocorrelation of the IR in (b).

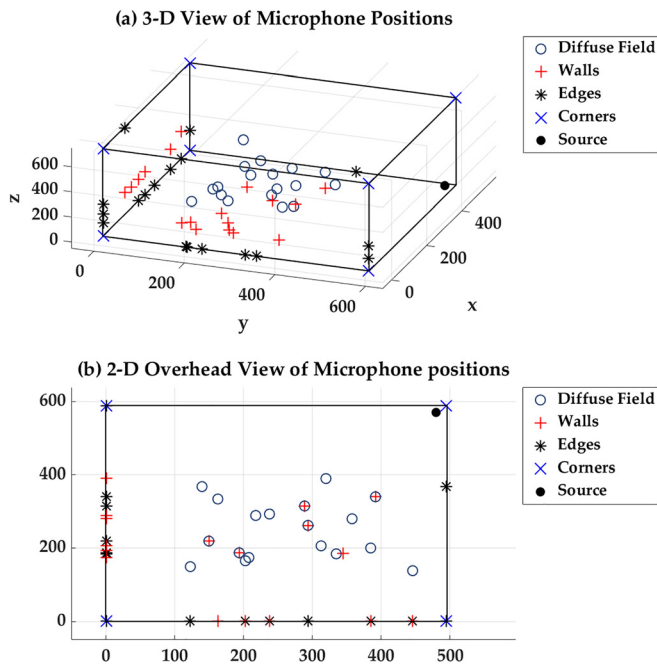


FIG. 9. (Color online) Receiver positions used in the numerical modeling. Each position region is denoted with a unique character. (a) 3-D representation of positions. (b) Top-down view of the chamber in 2-D.

calculations, and Fig. 10 shows the peak focal amplitudes obtained from the numerical model with a mean value for each region. The significance of the focal amplitude values lies in the uniformity of the focal amplitudes in each region and the difference in amplitudes from one region of focal locations to the next, as was investigated experimentally. The mean value (and one standard deviation above/below the mean) was measured to be 152.7 dB (+0.4/-0.5 dB) in the diffuse field, 155.7 dB (+0.4/-0.4 dB) against one wall, 159.1 dB (+0.2/-0.2 dB) against an edge (two walls), and 163.1 dB (+0.5/-0.6 dB) for the corners (three walls). The mean values increase by 3.0 dB (+0.3/-0.3 dB) when moving from the diffuse field to one wall, 3.4 dB (+0.2/-0.2 dB) when moving from one wall to an edge, and 4.0 dB (+0.4/-0.4 dB) when moving from the edge into a corner. The general trend of an increase in focal amplitude with the proximity to additional walls matches that seen experimentally.

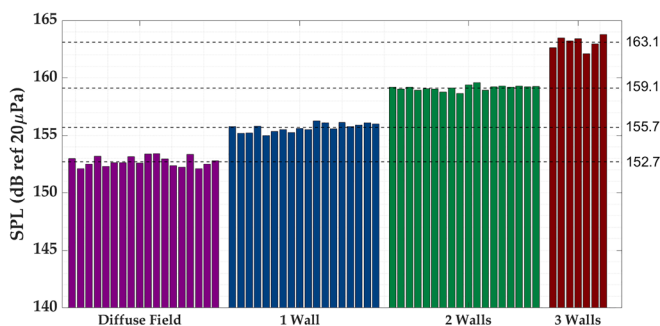


FIG. 10. (Color online) Bar graph display of measured peak SPL for various TR experiments done at the locations specified in Fig. 9 for the numerically modeled reverberation chamber. The mean of the peak SPL values for each region is displayed as a dashed line with mean value label to the right.

Numerical modeling was also conducted without using the previously mentioned filter that simulates the use of logarithmic chirp to see if this filter impacts the modeling results. The use of this filter to simulate the logarithmic chirp showed no significant change in the peak focal amplitudes generated by the model.

IV. COMPARISON OF NUMERICAL TO EXPERIMENTAL RESULTS

Table I provides a comparison summary of the two sets of experimental results in the SRC and in the LRC along with numerical results in the LRC. The comparison clearly shows that increasing the number of reflecting surfaces (walls) near the focal location consistently raises the value of the focus amplitude near an average of ≈ 3 dB per additional surface (to within the given standard deviation of each region). It is especially worth noting the overall uniformity of each region. Both of the experimental cases as well as the numerical case showed uniformity to within a very small deviation from the mean. This deviation was smallest in the numerical model, which is to be expected given the idealization of the algorithm’s “environment” (virtual space generated for calculation) when compared to the potential for systematic and random error in real world experimentation.

Variation in the increases (meaning comparing the 3.8 dB increase in the experimental LRC results to the 3.1 dB increase in the experimental SRC results to the 3.0 dB increase observed in the numerical LRC results when moving from the diffuse field region to the one-wall region) in average focal amplitude value from one focal location region to the next could be caused by multiple things. The loudspeakers used in the experiments are placed near walls, with the horn openings facing the wall, close enough that there could be a frequency-dependent change in the radiation from the source that is not seen in the numerical model (the model assumes sources with flat frequency responses). It is also worth noting that omnidirectional sources are assumed in the numerical model, whereas the experimental ones are directional. Because the experimental loudspeakers are directional, they were pointed away from the receiver to avoid the large direct path arrival relative to the other arrivals in the IR as suggested by Anderson *et al.*²⁶ The rooms used for experiments also had diffusor panels hung in them, whereas the numerical model assumed an empty rectangular room. Also, the number of sources used in the modeling was decreased to one to simplify the calculation. These exceptions aside, the increasing nature of the focal amplitude in each focal location region is consistent, and similar trends are seen in the experimental results and the numerical simulations.

V. THEORETICAL IMPACT OF WALL PROXIMITY ON FOCAL AMPLITUDE

Recall from Sec. III that traditional TR can be modeled as an autocorrelation of the IR. This is the equivalent to multiplying Eq. (1) by its complex conjugate to compute the auto-spectrum. The equation can be simplified by

TABLE I. Comparison of the average results for the increase in focal amplitude when the focal location is moved from one focal location region to the next (adding a wall each time) in each of the reverberation chambers as well as the numerical results. Values shown represent peak SPLs in decibels (ref 20 μPa). The average values for one-wall locations are given relative to the average diffuse field location values. The values for edge locations are given relative to the average one-wall values. The values for corner locations are given relative to the average edge location values. Values in parentheses represent one standard deviation above and below the mean pressure value given.

Focal location	Experimental LRC	Experimental SRC	Numerical LRC
Diffuse field	0.0 dB (+1.0/−1.4 dB)	0.0 dB (+0.5/−0.5 dB)	0.0 dB (+0.4/−0.5 dB)
Wall	+3.8 dB (+1.0/−1.2 dB)	+3.1 dB (+0.6/−0.7 dB)	+3.0 dB (+0.3/−0.3 dB)
Edge	+2.2 dB (+1.0/−1.2 dB)	+2.1 dB (+0.7/−0.8 dB)	+3.4 dB (+0.2/−0.2 dB)
Corner	+2.4 dB (+0.9/−1.1 dB)	+3.0 dB (+0.6/−0.7 dB)	+4.0 dB (+0.4/−0.4 dB)

condensing all of the terms not associated with the eigenfunctions into a single variable A_n ,

$$A_n = \frac{(k^2 - k_n^2 - j2k_n \frac{\delta_n}{c}) \Lambda_n}{-jk \rho_0 c Q / V}. \tag{5}$$

An auto-spectrum can then be represented by the product of the original summation with its complex conjugate,

$$y(r_0, r, k) = \sum_{n=0}^{\infty} \frac{G_n(r_0, r)}{A_n} \cdot \sum_{n=0}^{\infty} \frac{G_n(r_0, r)}{A_n^*}, \tag{6}$$

where $G_n(r_0, r)$ represents the product of the eigenfunctions $\Psi_n(x_0, y_0, z_0) \Psi_n(x, y, z)$ and in the case of a rigid walled room is a real quantity. This product of summations can then be expanded as

$$y(r_0, r, k) = \left(\dots + \frac{G_{n-1}(r_0, r)}{A_{n-1}} + \frac{G_n(r_0, r)}{A_n} + \frac{G_{n+1}(r_0, r)}{A_{n+1}} + \dots \right) \cdot \left(\dots + \frac{G_{n-1}(r_0, r)}{A_{n-1}^*} + \frac{G_n(r_0, r)}{A_n^*} + \frac{G_{n+1}(r_0, r)}{A_{n+1}^*} + \dots \right). \tag{7}$$

A careful analysis of the product of the summations allows them to be rewritten as the sum of same-indexed terms and a sum of cross-terms (where the indices are different),

$$y(r_0, r, k) = \sum_{n=0}^{\infty} \frac{G_n(r_0, r)^2}{|A_n|^2} + \sum_{l \neq m=0}^{\infty} \sum_{m \neq l=0}^{\infty} \frac{G_l(r_0, r) G_m(r_0, r)}{A_l A_m^*}. \tag{8}$$

The pressure contribution from a single mode can be evaluated as a fixed source while the receiver is moved throughout the space. Thus, the impact on the response from each mode when having the receiver against one or more walls may be determined. For any given mode, the first summation term in Eq. (8) yields an average increase in 6 dB when the receiver position is moved from the diffuse field region to up against one wall. Another 6 dB is gained when the receiver position is placed at an edge. And again, there is another 6 dB increase when the receiver position is in the

corner. The second summation term yields no average increase whether the receiver is in the diffuse field or up against any walls. Thus, when summing many modes in Eq. (8), the overall result is that a 6 dB increase should be expected when the receiver is placed exactly against each additional wall.

This analysis suggests a higher increase at the surface regions than is found both experimentally and numerically. This is likely due to the positions of the microphones being 0.01 m from the walls in both the experiments and the numerical simulation. Experimentally, this was done to avoid direct contact with the surfaces, so that mechanical vibration between the walls and the microphone would be avoided. Also, placing the microphones exactly in the corner or at an edge of a room is not possible due to the practical, finite size of microphones. The microphone positions used in the numerical calculation were mostly the same as in experiments in order to replicate the experiment as closely as possible with the numerical simulation. However, when the microphone positions are moved exactly against the walls in the simulation, the increase is 6 dB for each wall added, just as the mathematics in this section suggests.

VI. CONCLUSIONS

The results presented in this paper have shown that, using the TR process, a relative uniformity of the peak focal amplitude may be expected within a diffuse field (or when against one wall, against two walls, or against three walls). The standard deviation of the obtained focal amplitudes across each type of focal amplitude region is small. This indicates that no matter where a receiver is placed within a specific region (diffuse field, single wall, etc.), the amplitude may not fluctuate more than 1 dB. As described in Sec. II B, diffuse field theory predicts a deviation in SPL for any given frequency of up to 11 dB (+5/−6 dB above and below the mean) across a reverberant space.²³ The TR technique provides a peak focal amplitude that varies far less across a reverberant space, having a deviation of up to 1 dB (+0.5/−0.5 above and below the mean) experimentally and 0.9 dB (+0.4/−0.5 above and below the mean) in the modeling results.

The proximity of the focal location with respect to adjacent walls has a significant effect on the amplitude of a generated focus. The increase in amplitude expected when the focal location is placed exactly against each additional wall

is 6 dB. However, according to the presented experimental results, an increase in amplitude on the order of ≈ 3 dB per wall can be seen as the focal location is made to be adjacent to each additional wall, likely due to the practical inability to place a microphone exactly against a wall, edge, or corner of a room. This indicates that placement near three walls (in a corner of a room) produces the highest possible TR focal amplitude, approximately 9 dB higher than focal amplitudes obtained in the diffuse field. These experimental results are verified with a numerical model. This knowledge is important for the use of TR in reverberant environments.

These conclusions are based on experiments conducted in a SRC (volume 61 m^3) and in a LRC (volume 204 m^3). The full TR process (both forward and backward steps) was conducted for several different focal locations within these rooms while keeping the loudspeaker locations fixed. The focal locations included many positions away from walls in the diffuse field, near one wall, near two walls (edges of the room), and near three walls (corners of the room). A numerical model of the LRC was constructed to simulate TR in a rectangular room. The model was based on normal mode summation theory.

The size of a room also has an effect on the amplitude of the TR focusing. The facilities used in this study differed in volume by approximately a 3:1 ratio. The smaller of the two chambers produces focal amplitudes that average 2.4 dB higher for each type of focal location region. This agrees with the finding by Denison and Anderson²⁰ that a smaller volume room can contribute to the generation of a higher focal amplitude than a larger volume room.

ACKNOWLEDGMENTS

Funding provided by internal support from the Brigham Young University College of Physical and Mathematical Sciences is gratefully acknowledged. We thank Kevin Leete and Mylan Cook for their insight into mean and standard deviation calculations of pressure magnitudes.

¹M. Fink, "Time reversed acoustics," *Phys. Today* **50**(3), 34–40 (1997).
²B. E. Anderson, M. Griffa, C. Larmat, T. J. Ulrich, and P. A. Johnson, "Time reversal," *Acoust. Today* **4**(1), 5–16 (2008).
³C. S. Clay and B. Anderson, "Matched signals: The beginnings of time reversal," *Proc. Meet. Acoust.* **12**(1), 055001 (2011).
⁴A. Parvulescu and C. S. Clay, "Reproducibility of signal transmissions in the ocean," *Radio Electron. Eng.* **29**(4), 223–228 (1965).
⁵H.-C. Song, "An overview of underwater time-reversal communication," *IEEE J. Ocean. Eng.* **41**(3), 644–655 (2016).
⁶A. Sutin and H. Salloum, "Prospective medical applications of nonlinear time reversal acoustics," *Proc. Meet. Acoust.* **34**(1), 020003 (2018).
⁷G. Montaldo, P. Roux, A. Derode, C. Negreira, and M. Fink, "Ultrasound shock wave generator with one-bit time reversal in a dispersive medium, application to lithotripsy," *Appl. Phys. Lett.* **80**, 897–899 (2002).
⁸B. E. Anderson, M. Griffa, T. J. Ulrich, P.-Y. L. Bas, R. A. Guyer, and P. A. Johnson, "Crack localization and characterization in solid media using time reversal techniques," in *Proceedings of the 44th U.S. Rock Mechanics Symposium and 5th U.S.-Canada Rock Mechanics Symposium*, Salt Lake City, UT (June 27–30, 2010), ARMA-10-154.
⁹S. M. Young, B. E. Anderson, S. M. Hogg, P.-Y. L. Bas, and M. C. Remillieux, "Nonlinearity from stress corrosion cracking as a function of

chloride exposure time using the time reversed elastic nonlinearity diagnostic," *J. Acoust. Soc. Am.* **145**(1), 382–391 (2019).
¹⁰B. E. Anderson, L. Pieczonka, M. C. Remillieux, T. J. Ulrich, and P.-Y. L. Bas, "Stress corrosion crack depth investigation using the time reversed elastic nonlinearity diagnostic," *J. Acoust. Soc. Am.* **141**(1), EL76–EL81 (2017).
¹¹C. S. Larmat, R. A. Guyer, and P. A. Johnson, "Time-reversal methods in geophysics," *Phys. Today* **63**(8), 31–35 (2010).
¹²J. V. Candy, D. H. Chambers, C. L. Robbins, B. L. Guidry, A. J. Poggio, F. Dowla, and C. A. Hertzog, "Wideband multichannel time-reversal processing for acoustic communications in highly reverberant environments," *J. Acoust. Soc. Am.* **120**(2), 838–851 (2006).
¹³J. V. Candy, A. W. Meyer, A. J. Poggio, and B. L. Guidry, "Time-reversal processing for an acoustic communications experiment in a highly reverberant environment," *J. Acoust. Soc. Am.* **115**(4), 1621–1631 (2004).
¹⁴S. Yon, M. Tanter, and M. Fink, "Sound focusing in rooms: The time-reversal approach," *J. Acoust. Soc. Am.* **113**(3), 1533–1543 (2003).
¹⁵C. B. Wallace and B. E. Anderson, "High-amplitude time reversal focusing of airborne ultrasound to generate a focused nonlinear difference frequency," *J. Acoust. Soc. Am.* **150**(2), 1411–1423 (2021).
¹⁶J.-L. Thomas, F. Wu, and M. M. Fink, "Time reversal focusing applied to lithotripsy," *Ultrason. Imaging* **18**(2), 106–121 (1996).
¹⁷G. Ribay, J. de Rosny, and M. Fink, "Time reversal of noise sources in a reverberation room," *J. Acoust. Soc. Am.* **117**(5), 2866–2872 (2005).
¹⁸C. Draeger and M. Fink, "One-channel time-reversal in chaotic cavities: Theoretical limits," *J. Acoust. Soc. Am.* **105**(2), 611–617 (1999).
¹⁹A. Derode, A. Tourin, and M. Fink, "Limits of time-reversal focusing through multiple scattering: Long-range correlation," *J. Acoust. Soc. Am.* **107**(6), 2987–2998 (2000).
²⁰M. H. Denison and B. E. Anderson, "Time reversal acoustics applied to rooms of various reverberation times," *J. Acoust. Soc. Am.* **144**(6), 3055–3066 (2018).
²¹J. B. Allen and D. A. Berkley, "Image method for efficiently simulating small-room acoustics," *J. Acoust. Soc. Am.* **65**(4), 943–950 (1979).
²²F. Ma, J. Chen, J. H. Wu, and H. Jia, "Realizing broadband sub-wavelength focusing and a high intensity enhancement with a spacetime synergetic modulated acoustic prism," *J. Mater. Chem. C* **8**(28), 9511–9519 (2020).
²³F. Ma, J. Chen, and J. H. Wu, "Experimental study on performance of time reversal focusing," *J. Phys. D Appl. Phys.* **53**(5), 055302 (2020).
²⁴M. Kleiner and J. Tichy, *Acoustics of Small Rooms* (CRC, New York, 2017), pp. 37–99.
²⁵M. L. Willardson, B. E. Anderson, S. M. Young, M. H. Denison, and B. D. Patchett, "Time reversal focusing of high amplitude sound in a reverberation chamber," *J. Acoust. Soc. Am.* **143**(2), 696–705 (2018).
²⁶M. K. Rollins, T. W. Leishman, J. K. Whiting, E. J. Hunter, and D. J. Eggett, "Effects of added absorption on the vocal exertions of talkers in a reverberant room," *J. Acoust. Soc. Am.* **145**(2), 775–783 (2019).
²⁷M. R. Schroeder, "The 'Schroeder frequency' revisited," *J. Acoust. Soc. Am.* **99**(5), 3240–3241 (1996).
²⁸B. E. Anderson, M. Clemens, and M. L. Willardson, "The effect of transducer directivity on properties of time reversal focusing," *J. Acoust. Soc. Am.* **139**(4), 2083–2083 (2016).
²⁹B. Van Damme, K. Van Den Abeele, Y. Li, and O. Bou Matar, "Time reversed acoustics techniques for elastic imaging in reverberant and non-reverberant media: An experimental study of the chaotic cavity transducer concept," *J. Appl. Phys.* **109**, 104910 (2011).
³⁰H. Kuttruff, *Room Acoustics*, 6th ed. (CRC, Boca Raton, FL, 2017), pp. 66–69.
³¹M. R. Schroeder and K. H. Kuttruff, "On frequency response curves in rooms: Comparison of experimental, theoretical, and Monte Carlo results for the average frequency spacing between maxima," *J. Acoust. Soc. Am.* **34**(1), 76–80 (1962).
³²ISO 3741:2010, "Sound power and energy in reverberant environments" (International Organization for Standardization, Geneva, Switzerland, 2010).
³³M. R. Schroeder, "New method of measuring reverberation time," *J. Acoust. Soc. Am.* **37**(3), 409–412 (1965).
³⁴M. Tanter, J. Thomas, and M. Fink, "Time reversal and the inverse filter," *J. Acoust. Soc. Am.* **108**(1), 223–234 (2000).